Journal of Applied Mechanics and Technical Physics, Vol. 46, No. 5, pp. 691–696, 2005

THERMOCAPILLARY VORTICES INDUCED BY A LIGHT BEAM NEAR A BUBBLE SURFACE IN A HELE-SHAW CELL

N. A. Ivanova and B. A. Bezuglyi

UDC 535.21; 532.68

This paper studies thermocapillary vortices induced by local heating of a bubble surface in a Hele-Shaw cell by a light beam. It is found that the vortex rotation frequency and its depth depend on the distance from the light-beam projection onto the layer to the bubble boundary. The surface velocity of the thermocapillary flow is calculated using the balance of the near-surface and return flows of the thermocapillary vortex and the equality of capillary and dynamic pressures. It is shown that a decrease in the surface velocity and the vortex rotation frequency with increase in the distance from the light beam to the bubble surface is due to a decrease in the temperature gradient between the illuminated and cold poles of the bubble.

Key words: *bubble, thermocapillary flows, additivity of surface curvature, thermocapillary vortices, microfluidics.*

Introduction. Bubble motion in a Hele-Shaw cell ($h/D \ll 1$, where D is the bubble diameter and h is the cell spacing) has been extensively studied both theoretically and experimentally [1–4]. Recently, interest in this problem has increased because of the need to develop methods for controlling liquids and bubbles in microscale bubble pumps, biochips, etc. [5, 6]. However, for duct flows, the examined mechanisms of bubble motion due to mechanically produced pressure gradients [1–3] or the buoyancy forces arising from the cell inclination [4] are inefficient or do not operate altogether. For example, for ethanol drops ($\rho = 800$ kg/m^3 and $\sigma = 22.8 \cdot 10^{-3}$ N/m [7]) moving at a velocity of 1 cm/sec inside a microchannel with a cross-sectional size of 100 μm, the Bond number and the capillary number have orders of magnitude Bo $\approx 10^{-3}$ and Ca $\approx 10^{-4}$, respectively. That small values indicate that in the problems considered, capillary forces dominate over gravitational and viscous forces.

The migration of bubbles under the action of thermocapillary forces was first demonstrated by Young et al. [8], who studied bubble motion under the action of a vertical temperature gradient ∇T opposite to the buoyancy force. Mazouchi and Homsy [9] and Lajeunesse and Homsy [10] performed experimental and theoretical studies of bubble motion in polygonal microchannels under the action of thermocapillary forces related to a longitudinal temperature gradient [9, 10].

The possibility of controlling bubbles in a Hele-Shaw cell by means of a local temperature gradient induced by the thermal action of a light beam was first shown by Bezuglyi [11]. Later, Bezuglyi and Ivanova [12] reported results from studies of bubble motion behind a light beam and for the first time gave a qualitative explanation of the motion mechanism based on the action of localized thermocapillary liquid vortices induced by the light beam at the lateral surface of the bubble.

In the present work, an attempt was undertaken to obtain quantitative information on the size of thermocapillary vortices induced by the thermal action of light, the frequency of their rotation and flow velocity on the bubble surface.

Tyumen' State University, Tyumen' 625003; nivanova@utmn.ru. Translated from Prikladnaya Mekhanika i Tekhnicheskaya Fizika, Vol. 46, No. 5, pp. 93–99, September–October, 2005. Original article submitted July 12, 2004; revision submitted January 24, 2005.

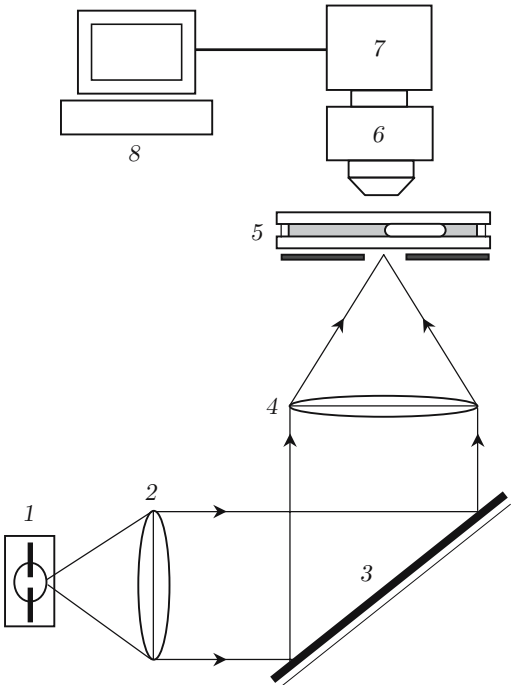

Fig. 1. Diagram of setup: 1) light source; 2) collector; 3) mirror; 4) condenser; 5) cell; 6) microscope; 7) video camera; 8) computer.

1. Experimental Procedure. A diagram of the setup is shown in Fig. 1. The point source of light was an HBO-100 mercury lamp with an optical beam-focusing system consisting of a collector lens, a rotary mirror, and a condenser lens. The diameter of the light beam in the focal plane was $d = 0.6 \pm 0.05$ mm, and the total beam power was 200 mW. The Hele-Shaw cell was located on the stage of a microscope equipped with a video camera (25 frames/sec; 560 lines/mm) connected through an Aver Media VC-8139 TV-tuner with a computer for frame-by-frame processing of the results.

The cell consisted of two quartz plates separated by a Teflon lining 50 μm thick with a rectangular 0.4×2.0 cm cavity, in which a few liquid drops were brought using a pipette. As a rule, the liquid was distributed in such a manner that a few bubbles of various diameters remained in the cell. The experiments were performed only with large bubbles for which the ratio of their diameters to the diameter of the light-beam projection onto the layer was $D^* \geqslant 1$.

The examined liquids were solutions of copper bromide in ethanol and acetone. The solution concentrations were such that the radiation absorption was sufficient to induce the thermocapillary effect (about 20% of the beam power).

Because the liquid surface tension was small ($\sigma = 22.8$ mN/m for ethanol and 23.7 mN/m for acetone at 20°C [7]), the effect of surfactant impurities on the thermocapillary flow was ignored. In addition, since appreciable changes in the volume bubble were not observed during the experiments, the evaporation and heating of the bubble gas was also ignored.

Before the experiment, the cell was placed on the microscope stage so that the boundary of any bubble was in the region of the light-beam projection or at a distance equal to its diameter (see Fig. 1). Then, the cell was moved on the stage at a velocity of 1 to 5 mm/sec in an arbitrary direction relative to the light beam. The bubble moved in the opposite direction, tending to occupy a position in the region of the beam projection. The bubble motion mechanism is due to the action of thermocapillary forces on its surface. These forces results from a decrease in the liquid surface tension [$\sigma = \sigma_0 + \sigma'_T(T - T_0)$] near the bubble due to local heating by the light beam [12]. Here $\sigma'_T < 0$ is the temperature coefficient of surface tension and σ_0 and T_0 are the initial surface tension and temperature. The thermocapillary forces cause the liquid to flow over the surface from the illuminated zone to its cold regions (Fig. 2). Owing to viscosity, the adjacent liquid layers are entrained in the thermocapillary flow,

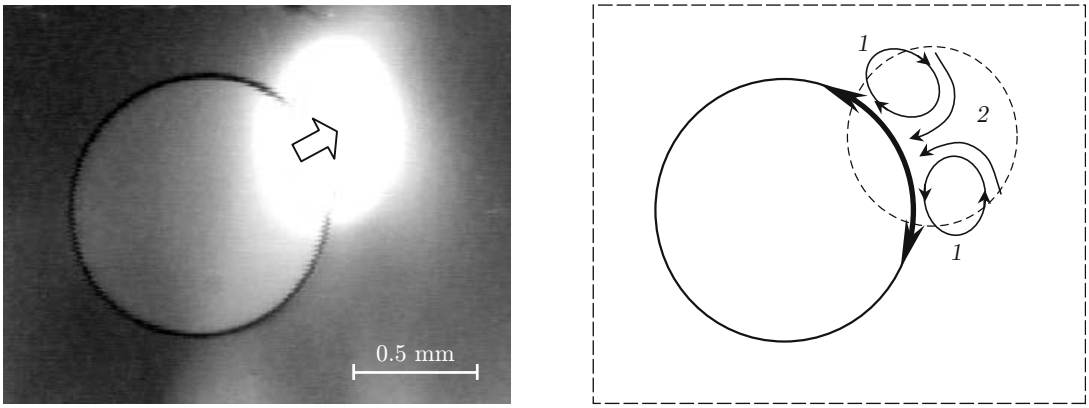

Fig. 2. Thermocapillary mechanism of bubble motion: the bubble follows the light beam in the cell ($h = 50$ μm) filled with a $CuBr_2$ solution in ethanol; 1) flow diagram on the surface and in the liquid volume, 2) light-beam projection; the arrow shows the direction of bubble motion.

resulting in removal of the liquid from the illuminated zone, and, hence, deformation of the equilibrium surface. This deformed surface produces an excess capillary pressure in the bubble:

$$P_\sigma = \sigma H_d.$$

Here H_d is the dynamic curvature, which, according to the additivity property of curvatures [13], is linked to the total curvature H and the bubble curvature in the state of rest H_s by the relation

$$H_d = H - H_s. \tag{1}$$

The negative-pressure region that arose under the deformed surface causes return flows, generating two consistent convective vortices (Fig. 2), which act as a motor that sets the bubble in motion.

2. Vortex Visualization. To experimentally study the localized liquid vortices at the bubble lateral surface and measure their quantitative characteristics, we used tracer particles which were the flakelike products of the reaction of fuchsine with copper bromide. Although this approach is not quite correct from the viewpoint of purity of the experiment, it was justified since the use of aluminum powder (whose average particle size was larger than 10 μm) as tracers in cells 50 μm thick led to the formation of particle clusters and, as a consequence, to flow blocking. The use of flakes had no marked effect on the flow and provides a clear picture of the convective vortices at the bubble surface due to local heating.

During the experiments, we estimated the rotation frequency of the vortices by fixing particle positions along streamlines in the sequence of frames obtained by cutting the video file using the ACDSee v4.0 program. In addition, we measured the bubble diameters in the state of rest and the total curvature of the illuminated bubble surface using the procedure described below.

3. Measurement of Vortex Characteristics. For a quantitative description of thermocapillary vortices, we introduce the notion of the vortex depth (w), which is defined as the diameter of the circular streamline that is directly adjacent to the surface and is bounded by the area of the light spot (Fig. 3a). This choice is motivated, first, by the fact that the flow along this line has the maximal velocity and, second, it is easy to trace the position of tracer particles to measure the vortex rotation frequency f. Below, we assume that the return flows extend beyond the beam. Visualization showed that the rotation frequency and depth of the vortices depend on the distance between the light beam and the bubble boundary. Figure 3 gives a sequence of video frames of thermocapillary vortices for various positions of the light beam from the bubble boundary.

When the beam is projected onto the bubble boundary, the vortex is localized in immediate proximity to it, and a small volume of the liquid is set in motion. In this case, the vortex depth is small and its rotation frequency is maximal. In Fig. 3a, the vortex depth is $w \leqslant 0.5d$, the vortex rotation frequency f reaches 12 sec^{-1}. If the light beam is at a certain distance from the bubble boundary, so that it covers only a small segment of the boundary, then the value of w increases and the value of f decreases compared to the previous situation. In Fig. 3b, the center of the beam projection is separated from the boundary by a distance equal to its radius; in this case, $w \simeq d$ and

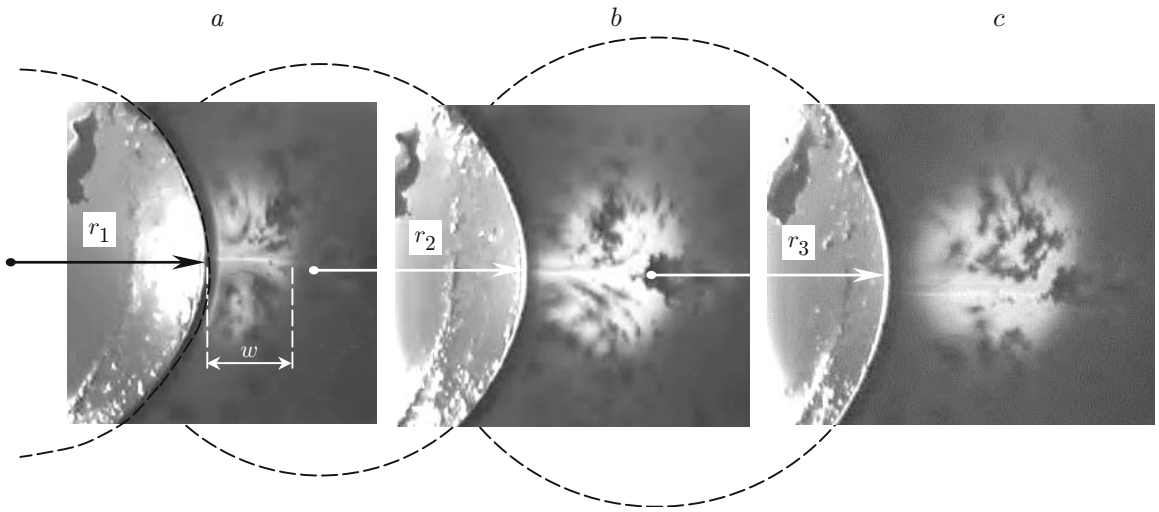

Fig. 3. Sequence of frames showing the variation in the depth of a thermocapillary vortex w with distance between the light beam and the bubble boundary: (a) the beam overlaps the bubble boundary; (b) the beam is at a distance of the order of its radius; (c) at a distance of the order of its diameter; $CuBr_2$ solution in acetone ($h = 50$ μm); the bubble is attached to the cell walls.

TABLE 1

Figure number	w, mm	v, mm/sec	v_s, mm/sec ($Q_- = Q_+$)	v_s, mm/sec ($P_i = P_\sigma$)	δv_s, %
3a	0.6 ± 0.1	22.6 ± 4.2	105.5 ± 37.0	148 ± 15	18
3b	0.9 ± 0.2	17.5 ± 3.6	73.5 ± 24.5	136 ± 10	42
3c	1.3 ± 0.3	9.5 ± 4.0	42.9 ± 29.0	119 ± 22	47

the frequency f decreases to 4–6 sec^{-1}. If the light beam is projected onto the layer at a distance approximately equal to the bubble diameter, the vortices lose their usually localized shape and their rotation frequency does not exceed the value $f \leqslant 1$ sec^{-1} (Fig. 3c).

Thus, the experiments revealed the inverse relationship between the rotation frequency and the vortex depth:

$$f \propto 1/w.$$

The frames obtained clearly show the dependence of the curvature radius of the illuminated surface r on the distance from this to the light-beam projection. Assuming that the deformed surface is a segment of a certain circle, we completed this circle on the frames and measured the radius of its curvature (see Fig. 3). It turned that as the distance between the light-beam projection and the bubble surface increases, the inequality $r_1 < r_2 < \ldots < r_n$ is satisfied, which implies that in the illuminated zone, the surface curvature is inversely proportional to the vortex depth, $H \propto 1/w$. Thus, for the sequence of frames presented in Fig. 3, the curvature radii are equal to $r_1 = (1.2 \pm 0.5)$ mm, $r_2 = (1.3 \pm 0.5)$ mm, and $r_3 = (1.5 \pm 0.5)$ mm for $w_1 < w_2 < w_3$ (the values of w_1, w_2, and w_3 are given in Table 1).

We note that if the beam is projected onto the layer at a distance from the bubble larger than the beam diameter, the bubble surface curvature in the illuminated zone becomes equal to its curvature in the state of rest, and vortical motion of the liquid is not observed. In this case, the bubble performs translational motion toward the light beam, which, in essence, is equivalent to classical thermocapillary bubble motion in a longitudinal temperature gradient [8, 14]. Then, as soon as the distance between the bubble surface and the light beam decreases to approximately the beam diameter, the occurrence of localized vortices is observed again.

4. Estimation of the Thermocapillary Flows Velocity near the Bubble Surface. The experiments showed that the thermocapillary vortices are asymmetric — their centers are shifted toward the interface (see Fig. 3). Thus, the cross-sectional area S_- of the flow adjoining the surface and spreading over it is smaller than the cross-sectional area S_+ of the return flow. Hence, based on the flux balance for closed vortical flow ($Q_- = Q_+$ or

$v_s S_- = v S_+$), the velocity of the thermocapillary liquid flow v_s is higher than the velocity of the return flow v for any distance from the light spot to the bubble surface.

The values of v estimated from the time variation in the tracer-particle position in the return flow varied in the range of 6 to 30 mm/sec, and the values of v_s obtained from the expression

$$v_s = v S_+ / S_-$$

are 14–140 mm/sec (see Table 1). We emphasize that the calculations took into account the total area of the return flow, which was slightly larger than that bounded by the vortex depth.

The approach based on the flux balance allows one to estimate the thermocapillary-flow velocity only when vortex visualization is possible. A different approach to determining v_s is based on the pressure balance and the additivity property of the curvature of the bubble lateral surface. The dynamic pressure $P_i = \rho v_s^2/2$ produced by the capillary liquid flow is compensated by the excess capillary pressure in the bubble $P_\sigma = \sigma H_d$. Consequently, the thermocapillary-flow velocity near the nonequilibrium surface is given by

$$v_s = \sqrt{2\sigma H_d/\rho} \tag{2}$$

and is linked to the dynamic curvature H_d, which is calculated by formula (1) using the known bubble curvature in the state of rest $1/r_s$ and the total curvature measured by the procedure described in Sec. 3.

Table 1 gives estimates of v_s obtained by formula (2) for the cases shown in Fig. 3 ($\rho = 790$ kg/m^3 and $\sigma = 23.7$ mN/m [7]) using the condition $H_s = \text{const}$. From the table it is evident that as the distance from the light beam to the bubble increases, the thermocapillary-flow velocity decreases, which is due to a decreases in the temperature gradient between the opposite poles of the bubble.

For a better understanding of the interrelation between the temperature gradient and the thermocapillary velocity, we use the condition of balance of the viscous stress and capillary force on the illuminated boundary of the bubble:

$$\mu \nabla v_x = \sigma_T' \nabla T. \tag{3}$$

Here μ is the viscosity of the liquid. The z coordinate is perpendicular to the tangent to the interface and points into the depth of the liquid, so that on the boundary, we have $v_x|_{z=s} = v_s$. We note that the value of v_s is maximal on the surface and decreases to zero at a distance of approximately $w/3$ (i.e., at the center of the vortex, we have $v_x|_{z=w/3} \simeq 0$), and the temperature varies along the bubble surface from the maximal value T_h at the illuminated pole of the bubble to T_0 at the cold pole. Then, the boundary condition (3) can be written as

$$3\mu v_s/w = 2\sigma_T' \Delta T/(\pi r_s),$$

whence

$$\Delta T = T_h - T_0 = 1.5\pi\mu v_s r_s/(\sigma_T' w). \tag{4}$$

For $r_s \simeq 2.40$ mm, $\mu = 0.32 \cdot 10^{-3}$ Pa$\cdot$sec, and $\sigma_T' = 0.11 \cdot 10^{-3}$ N/(m$\cdot$K) [7] and the values of v_s and w for Fig. 3a, 3b, and 3c (see Table 1), relation (4) gives estimates of ΔT equal 8, 5, and 3 K, respectively. From this, one can see that the temperature gradient indeed decreases considerably as the beam moves away and the temperature-gradient change between the initial and final positions of the beam is about 40%. The heat from the light beam at a distance from the bubble boundary is attenuated because of dispersion into the support and increases the bubble-surface temperature only slightly.

The relative error of the methods for estimating the velocity of the near-surface thermocapillary flow $\delta v_s = (v_s^{(Q)} - v_s^{(P)})/(v_s^{(Q)} + v_s^{(P)}) \cdot 100\%$ is presented in Table 1. The increase in the error with increase in the vortex depth can be caused by two factors. First, the method $Q_- = Q_+$ underestimates the values of S_+ because the vortex loses its typical localized shape: particles are accumulated in the light beam and are almost absent on the periphery. Second, the method $P_i = P_\sigma$ gives overestimated values of the curvature H_d and, hence, the velocity. This is due to the fact that to measure H_d, we completed the circle in the frame so that its arc covered only a minimal segment on the deformed surface. This restriction of the circle is explained by the limiting case $H \to H_s$, where it is difficult to visually detect the deformation of the equilibrium surface, and the construction of a circle that maximally describes the deformed surface gave zero or negative values of H_d in the calculations.

Conclusion. Frame-by-frame processing of video records of visualized vortex liquid flow at the illuminated bubble surface provided information on the size and rotation frequency of thermocapillary vortices. An approach

to determining the velocity of the near-surface thermocapillary flows was proposed based on measuring the total curvature of the bubble surface in the illuminated zone and its equilibrium curvature.

Results of the experiments showed that the depth and rotation frequency of the vortices induced by the light beam at the bubble surface depend on the distance from the light-beam projection to the bubble boundary. With increase in this distance, the depth of the vortices increases and the vortex rotation frequency, the near-surface thermocapillary flow velocity, and the total curvature H of the illuminated bubble surface ($H_s = \text{const}$) decrease.

This work was supported by the Russian Foundation for Basic Research (Grant No. 04-01-00493).

REFERENCES

1. G. I. Taylor and P. G. Saffman, "A note of the motion of bubbles in a Hele-Shaw cell and porous medium," *Quart. J. Mech. Appl. Math.*, **12**, 265 (1959).
2. A. R. Kopf-Sill and G. M. Homsy "Bubble motion in a Hele-Shaw cell," *Phys. Fluids*, **31**, No. 1, 18–26 (1988).
3. C. W. Park, S. K. Maruvada, and D. Y. Yoon, "The influence of surfactant on the bubble motion in Hele-Shaw cells," *Phys. Fluids*, **6**, No. 10, 3267–3275 (1994).
4. T. Maxworthy, "Bubble formation, motion and interaction in a Hele-Shaw cell," *J. Fluid Mech.*, **173**, 95 (1986).
5. T. K. Jun and C. J. Kim, "Valveless pumping using traversing vapor bubbles in microchannels," *J. Appl. Phys.*, **83**, No. 11, 5658–5664 (1998).
6. D. D. Cunningham, "Fluidics and sample handling in clinical chemical analysis," *Anal. Chim. Acta*, No. 429, 1–18 (2001).
7. A. Faghri, *Heat Pipe Science and Technology*, Tylor and Francis Washington, D. C. (1995).
8. N. O. Young, J. S. Goldstein, and M. J. Block, "The motion of bubbles in a vertical temperature gradients," *J. Fluid Mech.*, **6**, No. 3, 350–356 (1959).
9. A. Mazouchi and G. M. Homsy, "Thermocapillary migration of long bubbles in polygonal tubes, I. Theory," *Phys. Fluids*, **13**, No. 6, 1594–1600 (2001).
10. E. Lajeunesse and G. M. Homsy, "Thermocapillary migration of long bubbles in polygonal tubes II. Experiments," *Phys. Fluids*, **5**, No. 2, 308–314 (2003).
11. B. A. Bezuglyi, "Capillary convection controlled by the thermal action of light and its use in information recording," Doct. Dissertation (1983).
12. B. A. Bezuglyi and N. A. Ivanova, "Manipulation of a gas bubble in a Hele-Shaw cell using a light beam," *Pis'ma Zh. Tekh. Fiz.*, **28**, No. 19, 71–75 (2002).
13. B. A. Bezuglyi, O. A. Tarasov, and A. A. Fedorets, "Modified method of an inclined plate for measuring the limiting wetting angle," *Kolloid. Zh.*, **6**, 735–741 (2001).
14. G. Wozniak, R. Balasubramaniam, P. H. Hadland, and R. S. Subramanian, "Temperature fields in a liquid due to the thermocapillary motion of bubbles and drops," *Exp. Fluids*, No. 31, 84–89 (2001).